ADVANCED MATERIALS

Supporting Information

for *Adv. Mater.*, DOI: 10.1002/adma.201907995

Optimization of the Pore Structures of MOFs for Record High Hydrogen Volumetric Working Capacity

Xin Zhang, Rui-Biao Lin, Jing Wang, Bin Wang, Bin Liang, Taner Yildirim, Jian Zhang, Wei Zhou,* and Banglin Chen**

Supporting Information

Optimization of the Pore Structures of MOFs for Record High Hydrogen Volumetric Working Capacity

Xin Zhang,[a] Rui-Biao Lin,[a] Jing Wang,[ad] Bin Wang,[a] Bin Liang,[a] Taner Yildirim,[c] Jian Zhang,[b] Wei Zhou*[c] and Banglin Chen*[a]*

Dr. X. Zhang, Dr. R.-B. Lin, Prof. J. Wang, Dr. B. Wang, Dr. B. Liang, Prof. B. Chen
Departmentof Chemistry, University of Texas at San Antonio
One UTSA Circle, San Antonio,TX 78249-0698 (USA)
E-mail: banglin.chen@utsa.edu

Dr. J. Zhang
The Molecular Foundry, Lawrence Berkeley National Laboratory Berkeley, CA 94720 (USA)
E-mail: jianzhang@lbl.gov

Dr. T. Yildirim, Dr. W. Zhou
NIST Center for Neutron Research, Gaithersburg, Maryland 20899-6102 (USA)
E-mail: wzhou@nist.gov

Prof. J. Wang
College of Chemical Engineering, Zhejiang University of Technology.
Hangzhou 310014 (China)

Adsorption potential energy and pore geometry

The total adsorption potential energy is the sum of adsorbate-adsorbate potential and adsorbate-adsorbent potential: $\phi_{total} = \phi_{adsorbate-adsorbate} + \phi_{adsorbate-adsorbent}$. Since the adsorbate-adsorbate interaction is primarily related to adsorbate molecules. The adsorbate-adsorbent interaction is the study focus to improve the total potential energy. [1]

In reality, the guest molecule interacts with multiple atoms on the pore surface, and the adsorption potential is the sum of all interaction potential. The pore geometry affects the number of atoms interacting with guest molecule and subsequently the overall adsorbate-adsorbent potential. A comparison between slit, cylindrical, and spherical pore surface as shown in the bottom figures in Figure S1, the number of surface atoms interacting with guest molecules is highest in spherical pore and smallest in slit pore with flat surface. Therefore, the interaction potential in spherical pore is the highest and potential in slit pore is lowest. [2]

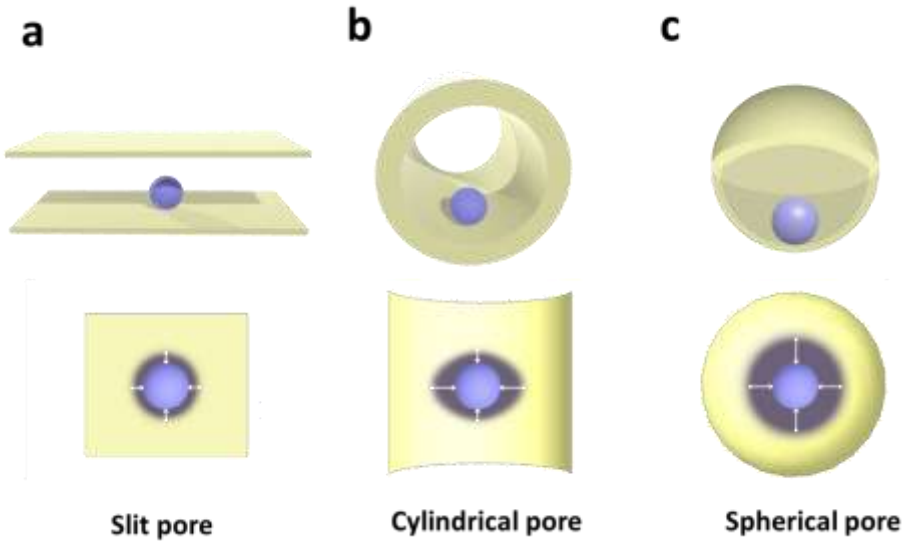

Figure S1. Cartoon of gas molecule (purple sphere) in three type of pores (yellow surface). The bottum figures demonstrate the detailed sobent-sorbate interaction between gas molecule and flat surface of slit pore (a), curve surface of cylindrical pore (b), and spherical pore surface (c). The shadow area indicates the region of pore surface interacting with the guest molecules.

Table S1. Hydrogen adsorption properties and deviation between measured/theoretical pore properties of MOFs investigated.

MOF	Density g/cm^3	Pore geometry type	Total adsorption (mmol/g)	Saturated adsorption (mmol/g)	Pore occupancy	Pore Volume (cm^3/g)			BET Surface Area m^2/g		
						Measured	Theoretical	Deviation of V_p	Measured	Theoretical	Deviation of S_{BET}
HKUST-1	0.879	cage	28.04	33.21	0.844	0.75	0.75	0 %	1980	1950	1.5 %
NOTT-112	0.503	cage	47.86	58.40	0.819	1.44	1.53	-5.88 %	3440	4046	-15.0 %
NU-125	0.578	cage	44.67	57.05	0.783	1.33	1.3	2.31 %	3230	3140	2.9 %
NU-1000	0.486	channel	43.38	63.86	0.679	1.48	1.6	-7.5 %	2200	2350	-6.4 %
UiO-68-Ant	0.608	cage	41	51.51	0.796	1.17	1.1	6.36 %	3030	2930	3.4 %
rht-MOF-7	0.789	cage	25.68	32.04	0.801	0.79	0.81	-2.47 %	1950	2270	-14.1 %
Cu-MOF-74	1.206	channel	16.26	20.01	0.813	0.47	0.49	-4.08 %	1270	1190	6.7 %
UiO-67	0.724	cage	31.14	36.90778	0.84372	0.91	0.89	2.25 %	2360	2910	-18.9 %
CYCU-3-Al	0.442	channel	44.92	63.27048	0.70997	1.56	1.64	-4.88 %	2450	2865	-14.5 %
$Zn_2(bdc)_2(dabco)$	0.828	channel	25.72	33.21	0.775	0.76	0.71	7.04 %	2020	1990	1.5 %

Fitting of pore occupancy vs pore volume and cross-validation

Six MOFs from single measurement with consistent experimental surface area and theoretical surface area, are used in pore occupancy fitting and cross-validation: HKUST-1; NU-125; UiO-68-Ant; NU-1000; $Zn_2(bdc)_2(dabco)$; Cu-MOF-74 as shown in Table S2.

Table S2. MOFs for the fitting of pore occupancy vs pore volume

MOF	Pore geometry type	Pore volume	Pore occupancy
HKUST-1	cage	0.78	0.84438
NU-125	cage	1.34	0.783
UiO-68-Ant	cage	1.21	0.79589
NU-1000	channel	1.5	0.67928
$Zn_2(bdc)_2(dabco)$	channel	0.78	0.77451
Cu-MOF-74	channel	0.47	0.8126

Pore occupancy was fitted as: $O = 0.992 - 0.149 \times V_p$ for cage-type MOFs $O = 0.881 - 0.128 \times V_p$ for channel-type MOFs. (Also see Figure 2a.)

To assess the justification of fitting in two categories: cage-type and channel-type MOFs, cross-validation was performed in two ways: 1. two separate sets of three MOFs: cage-type and channel-type; 2. one set of six MOFs. For each set of MOFs, one MOF was chosen as test set, and the rest of MOFs were fitting set. After the correlation was fitted with fitting set, the test set was used to evaluate the accuracy of the fitted equation. For example, in Table S3 No.1, HKUST-1 was choosen as test set, and the other two cage-type MOFs NU-125 and UiO-68-Ant are fitting set to obtain the equation $O = a \times V_p + b$ (O is pore occupancy, V_p is pore volume). Once the equation is fitted, the pore occupancy of HKUST-1 was predicted by the equation as 0.84147 which deviates from the acctual occupancy 0.84438 by -0.3 %.

As shown in Table S3, the deviation of test set prediction ranges from 0.1 % to 1.0 % if the MOFs are separated into two sets based on their pore geometry. In contrast, fitting six MOFs together lead to much higher deviation from 5.5 % to 15.0 % as shown in Table S4. Therefore, the catagorization of two sets of MOFs based on their pore geometry is more reasonable than fitting with all six MOFs together.

Table S3. Cross-validation of fitting for pore occupancy with two sets of MOFs: cage type and channel type of MOFs.

No.	MOFs type	a	b	Test set	Deviation % of test set
1	Cage	-0.0991	0.9158	HKUST-1	-0.3
2	Cage	-0.10541	0.92344	NU-125	-0.1
3	Cage	-0.10402	0.92239	UiO-68-Ant	0.1
4	Channel	-0.12285	0.87034	NU-1000	1.0
5	Channel	-0.12943	0.87343	$Zn_2(bdc)_2(dabco)$	-0.3
6	Channel	-0.13226	0.87768	Cu-MOF-74	0.4
-Fitting equation: pore occupancy $O = a \times V_p + b$; (V_p is the pore volume in cm^3/g) -Three cage-type MOFs used for cross-validation: HKUST-1;NU-125; UiO-68-Ant; -Three channel-type MOFs used for cross-validation: NU-1000; $Zn_2(bdc)_2(dabco)$; Cu-MOF-74					

Table S4. Cross-validation of fitting for pore occupancy with all six MOFs regarless of the pore geometry.

No.	a	b	Test set	Coefficient (R^2)	Deviation % of test set
1	-0.08154	0.85549	HKUST-1	0.43979	-5.9
2	-0.11777	0.89227	NU-125	0.59398	-6.2
3	-0.1086	0.88388	UiO-68-Ant	0.57683	-5.5
4	-0.03498	0.8339	NU-1000	0.20416	15.0
5	-0.10858	0.89747	$Zn_2(bdc)_2(dabco)$	0.55936	4.9
6	-0.12845	0.91876	Cu-MOF-74	0.51671	5.6
-Fitting equation: pore occupancy $O = a \times V_p + b$; (V_p is the pore volume in cm^3/g) -All six MOFs used for cross-validation: HKUST-1;NU-125; UiO-68-Ant; NU-1000; $Zn_2(bdc)_2(dabco)$; Cu-MOF-74					

Our empirical equations:

$n_{tot} = 42.22 \times V_p - 6.36 \times V_p^2$ *for* cage-type MOFs*;*

$n_{tot} = 37.49 \times V_p - 5.44 \times V_p^2$ for channel-type MOFs;

Cahine's rule:

$n_{tot} = 1.91 \times 10^{-3} \times SA \times 1000 \div 2.02 + 15.528 \times V_p$

$= 0.946 \times SA + 15.528 \times V_p$

n_{tot} is *in* mmol/g, V_p is pore volume in cm^3/g, and SA is BET surface area in m^2/g.

Scheme S1. Our empirical euqations and Cahine's rule to predict the H_2 total adsorption under 100 bar and 77 K.

Table S5. List of experimental H_2 total adsorption under 100 bar and 77 K, in comparison of predicted values by our equations and Cahine's rule.

MOFs	Pore volume (cm^3/g)	Surface area (m^2/g)	Pore geometry type	Measured total adsorption (mmol/g)	Predicted by our equations (mmol/g)	Deviation % of our equations	Predicted by Chahine's rule (mmol/g)	Deviation % of Chahine's rule
NU-1103	2.72	6245	cage	73.97	67.83	-8.30	101.29	36.93
NPF-200	2.17	5830	cage	65.723	61.85	-5.90	88.98	35.38
NU-1101	1.72	4340	cage	52	53.82	3.51	67.74	30.28
NU-1102	1.63	3720	cage	54.4	52.37	-3.74	60.80	11.76
CYCU-3-Al	1.56	2450	channel	44.92	45.26	0.76	47.39	5.50
NOTT-112	1.44	3440	cage	47.86	47.62	-0.49	54.89	14.68
MOF-5	1.3	3800	channel	43	40.94	-4.80	54.33	26.34
Uio-67	0.91	2360	cage	31.14	33.16	6.49	36.45	17.04
rht-MOF-7	0.79	1950	cage	25.68	29.39	14.45	30.71	19.57
**All above MOFs are not used for empirical equation fitting to validate our equations.								

Table S6. Experimental pore properties of some representative highly porous MOFs.

MOF	**Pore Volume (cm^3/g)**	**Pore geometry type**	**Gravimetric Surface Area (m^2/g)**	**Density (g/cm^3)**	**Volumetric Surface Area (m^2/cm^3)**	**Reference**
DUT-60	5.02	cage	7839	0.126	988	[3]
NU-110E	4.40	cage	7140	0.237	1692	[4]
NU-1103	2.91	cage	6550	0.298	1952	[5]
MOF-210	3.60	cage	6240	0.25	1560	[6]
NU-1104	2.79	cage	6230	0.291	1813	[5]
NU-100 (PCN-610)	2.82	cage	6143	0.303	1861	[7]
NPF-200	2.17	cage	5830	0.389	**2268**	[8]
UMCM-2	2.32	cage	5200	0.4	2080	[9]
NU-111	2.09	cage	4930	0.409	2016	[10]
NU-1102	2.00	cage	4830	0.403	1946	[5]
NU-1301	3.90	cage	4750	0.124	589	[11]
MOF-200	3.59	cage	4530	0.222	1006	[6]
MOF-205	2.16	cage	4460	0.382	1704	[6]
NU-1101	1.72	cage	4340	0.458	1988	[5]
Cu-tbo-MOF-5	1.12	cage	3971	0.595	2363	[12]
MOF-5	1.3	channel	3800	0.59	2242	[13]

Table S7. Pore properties of three major cavities in NPF-200

	Cavity-1	Cavity-2	Cavity-3
Diameter (Å)	19	13	11
Aperture (Å)	9.3	9	11
D/A	2	1.4	1

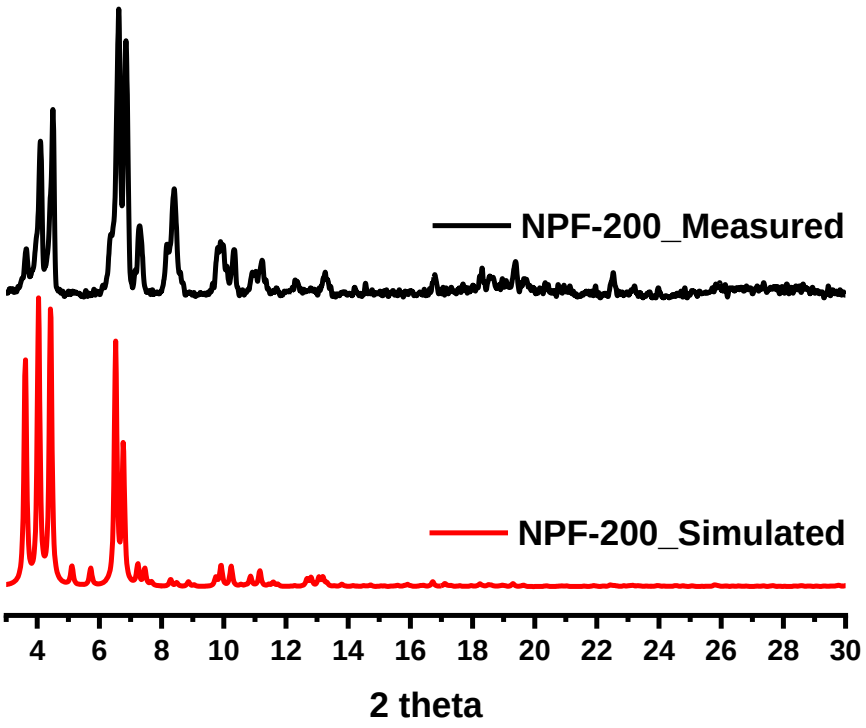

Figure S2. PXRD of NPF-200 and comparison with that simulated from single crystal structure.

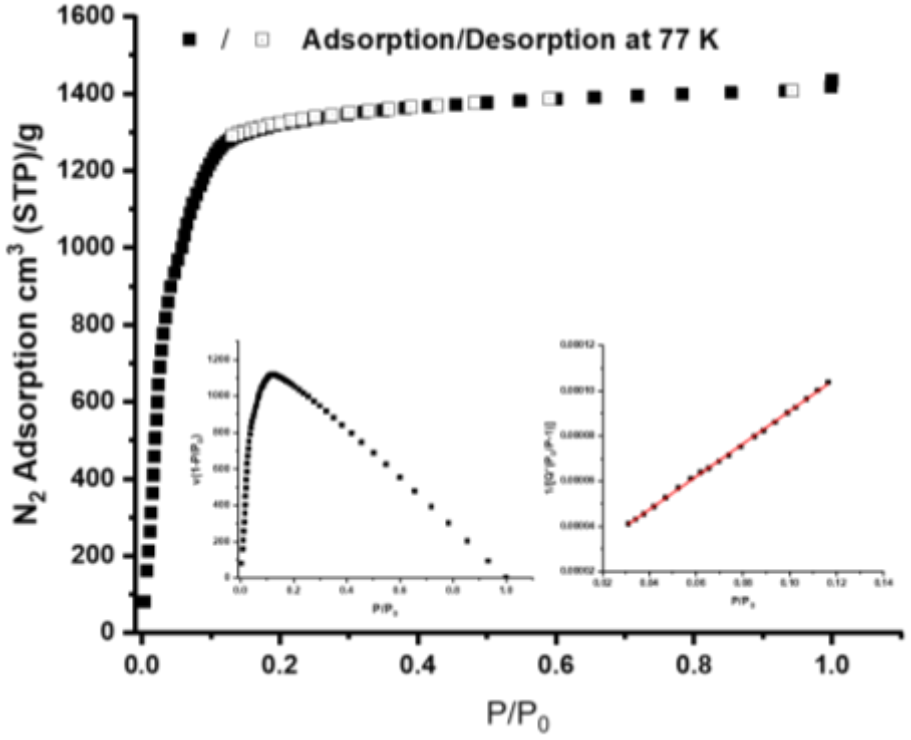

Figure S3. N_2 adsorption of NPF-200 at 77 K. BET surface area is calculated as 5830 m^2/g using pressure (P/P_0) range of 0.031 to 0.116 with fitting r^2= 0.99947.

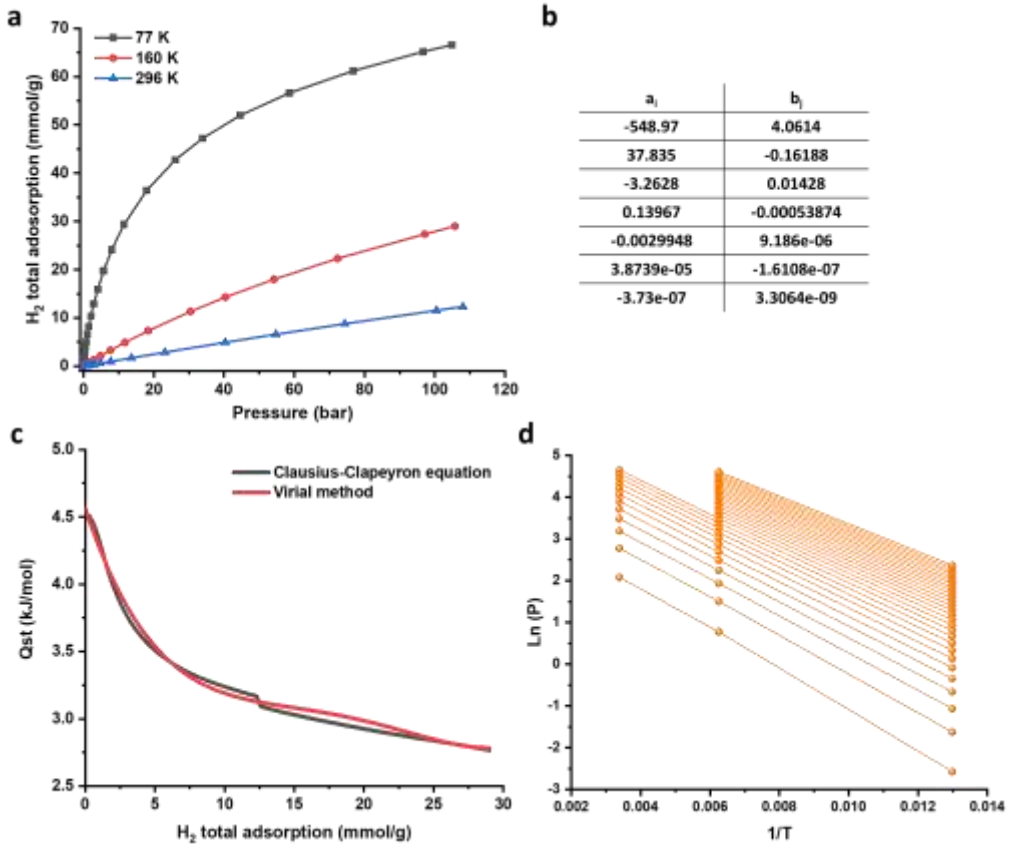

a_i	b_i
-548.97	4.0614
37.835	-0.16188
-3.2628	0.01428
0.13967	-0.00053874
-0.0029948	9.186e-06
3.8739e-05	-1.6108e-07
-3.73e-07	3.3064e-09

Figure S4. a) Hydrogen adsorption isotherms of NPF-200 at different temperatures. b) Fitting parameters for Virial equation: $Ln(P) = Ln\,(N) + \left(\frac{1}{T}\right)\sum_{i=0}^{m} a_i \times N^i + \sum_{j=0}^{n} b_j \times N^j$. c) Qst calculations by Virial method and Clausius-Clapeyron equation. d) The ln(P) vs 1/T plot.

Table S8. List of MOFs material and their pore volume, H_2 total adsorption and working capacity.

MOF	Pore volume (cm^3/g)	H_2 total adsorption (mmol/g)	Working capacity		References
			Gravimetric (wt %)	Volumetric (g/L)	
NPF-200	**2.18**	**65.72**	**8.7**	**37.2**	**This work**
HKUST-1	0.75	28.04	2.0	17	[14]
NOTT-112	1.44	47.86	5.3	24	[14]
NU-125	1.33	44.67	4.1	24	[14]
rht-MOF-7	0.79	25.68	1.8	14	[14]
Cu-MOF-74	0.47	16.26	1.0	13	[14]
PCN-250	0.71	28.35	1.8	16	[14]
NU-1000	1.48	43.38	5.2	30	[14]
UiO-67	0.91	31.14	2.9	20	[14]
UiO-68-Ant	1.17	41	4.3	26	[14]
CYCU-3-Al	1.56	44.92	5.5	27	[14]
$Zn_2(bdc)_2(dabco)$	0.76	25.72	1.6	14	[14]
NU-1101	1.72	52	6.1	30	[15]
NU-1102	1.65	54.4	6.9	31	[15]
NU-1103	2.72	73.97	10.1	33	[15]
MOF-5	1.36	43	4.5	31.1	[16]
IRMOF-20	1.65	Unavailable	5.7	33.4	[16]
SNU-70	2.14	Unavailable	7.8	34.3	[16]
UMCM-9	2.31	Unavailable	7.3	34.1	[16]
NU-100	3.17	Unavailable	10.1	35.5	[16]
*Total adsorption is measured under 100 bar and 77 K, working capacity is between 100 bar and 5 bar at 77K.					

References

[1] R. T. Yang, *John Wiley & Sons, Inc.: Hoboken, NJ*, **2003**.

[2] S. U. Rege, R. T. Yang, *AlChE J.* **2000**, 46, 734.

[3] I. M. Honicke, I. Senkovska, V. Bon, I. A. Baburin, N. Bonisch, S. Raschke, J. D. Evans, S. Kaskel, *Angew. Chem. Int. Ed.* **2018**, 57, 13780.

[4] O. K. Farha, I. Eryazici, N. C. Jeong, B. G. Hauser, C. E. Wilmer, A. A. Sarjeant, R. Q. Snurr, S. T. Nguyen, A. O. Yazaydin, J. T. Hupp, *J. Am. Chem. Soc.* **2012**, 134, 15016.

[5] T. C. Wang, W. Bury, D. A. Gomez-Gualdron, N. A. Vermeulen, J. E. Mondloch, P. Deria, K. Zhang, P. Z. Moghadam, A. A. Sarjeant, R. Q. Snurr, J. F. Stoddart, J. T. Hupp, O. K. Farha, *J. Am. Chem. Soc.* **2015**, 137, 3585.

[6] H. Furukawa, N. Ko, Y. B. Go, N. Aratani, S. B. Choi, E. Choi, A. O. Yazaydin, R. Q. Snurr, M. O'Keeffe, J. Kim, O. M. Yaghi, *Science* **2010**, 329, 424.

[7] a) O. K. Farha, A. O. Yazaydin, I. Eryazici, C. D. Malliakas, B. G. Hauser, M. G. Kanatzidis, S. T. Nguyen, R. Q. Snurr, J. T. Hupp, *Nat. Chem.* **2010**, 2, 944; b) D. Yuan, D. Zhao, D. Sun, H. C. Zhou, *Angew. Chem. Int. Ed.* **2010**, 49, 5357.

[8] X. Zhang, X. Zhang, J. A. Johnson, Y.-S. Chen, J. Zhang, *J. Am. Chem. Soc.* **2016**, 138, 8380.

[9] K. Koh, A. G. Wong-Foy, A. J. Matzger, *J. Am. Chem. Soc.* **2009**, 131, 4184.

[10] Y. Peng, G. Srinivas, C. E. Wilmer, I. Eryazici, R. Q. Snurr, J. T. Hupp, T. Yildirim, O. K. Farha, *Chem. Commun.* **2013**, 49, 2992.
[11] P. Li, N. A. Vermeulen, C. D. Malliakas, D. A. Gomez-Gualdron, A. J. Howarth, B. L. Mehdi, A. Dohnalkova, N. D. Browning, M. O'Keeffe, O. K. Farha, *Science* **2017**, 356, 624.
[12] I. Spanopoulos, C. Tsangarakis, E. Klontzas, E. Tylianakis, G. Froudakis, K. Adil, Y. Belmabkhout, M. Eddaoudi, P. N. Trikalitis, *J. Am. Chem. Soc.* **2016**, 138, 1568.
[13] S. S. Kaye, A. Dailly, O. M. Yaghi, J. R. Long, *J. Am. Chem. Soc.* **2007**, 129, 14176.
[14] P. García-Holley, B. Schweitzer, T. Islamoglu, Y. Liu, L. Lin, S. Rodriguez, M. H. Weston, J. T. Hupp, D. A. Gómez-Gualdrón, T. Yildirim, O. K. Farha, *ACS Energy Lett.* **2018**, 3, 748.
[15] D. A. Gomez-Gualdron, T. C. Wang, P. Garcia-Holley, R. M. Sawelewa, E. Argueta, R. Q. Snurr, J. T. Hupp, T. Yildirim, O. K. Farha, *ACS Appl. Mater. Interfaces* **2017**, 9, 33419.
[16] A. Ahmed, S. Seth, J. Purewal, A. G. Wong-Foy, M. Veenstra, A. J. Matzger, D. J. Siegel, *Nat. Commun.* **2019**, 10, 1568.